LAWRENCE
LIVERMORE
NATIONAL
LABORATORY

LLNL-JRNL-654185

The Impact of Laser Plasma Interactions on Three Dimensional Drive Symmetry in Inertial Confinement Fusion Implosions

J. L. Peterson, P. Michel, C. A. Thomas, R. P. J. Town

May 9, 2014

Physics of Plasmas

Disclaimer

The Impact of Laser Plasma Interactions on Three Dimensional Drive Symmetry in Inertial Confinement Fusion Implosions

J. L. Peterson,* P. Michel, C. A. Thomas, and R. P. J. Town
Lawrence Livermore National Laboratory, Livermore, California 94550, USA
(Dated: July 10, 2014)

Achieving symmetric hohlraum radiation drive is an important aspect of indirectly driven inertial confinement fusion experiments. However, when experimentally delivered laser powers deviate from ideal conditions, the resultant radiation field can become asymmetric. Two situations in which this may arise are random uncorrelated fluctuations in as-delivered laser power and laser beams that do not participate in the implosion (either intentionally or unintentionally). Furthermore, laser-plasma interactions in the hohlraum obfuscate the connection between laser powers and radiation drive. To study the effect of these situations on drive symmetry, we develop a simplified model for crossed-beam energy transfer, laser backscatter and plasma absorption that can be used in conjunction with view factor calculations to expediently translate laser powers into three-dimensional capsule flux symmetries. We find that crossed-beam energy transfer can alter both the statistical properties of uncorrelated laser fluctuations and the impact of missing laser beams on radiation symmetry. A method is proposed to mitigate the effects of missing laser beams.

I. INTRODUCTION

Understanding and controlling radiation drive symmetry is an important aspect of achieving ignition and gain in indirect drive laser inertial fusion experiments like those at the National Ignition Facility (NIF) [1]. In NIF experiments, 192 laser beams grouped into 48 4-beam "quads" enter a hohlraum through the laser entrance hole (LEH), propagate through the hohlraum cavity and strike the inner hohlraum surface. X-rays emitted from the hohlraum then bathe a capsule in radiation, causing ablation and compression [2, 3]. The symmetry of this radiation field has a direct impact on the symmetry of the implosion and the compressed fusion fuel, with asymmetric implosions undesirable.

Achieving ignition and gain necessitates meeting stringent requirements on capsule flux symmetry [4, 5]. This means that the laser power must be delivered to within a certain specification (usually a few percent). However, as the lasers propagate from the LEH, they interact with the plasma inside of the hohlraum. These laser plasma interactions can alter the amount of flux delivered to the hohlraum wall by a particular laser beam. Specifically, crossed-beam energy transfer [6, 7] at the LEH, whereby laser energy can be effectively transferred between beams through plasma waves, can strongly affect drive and capsule symmetry [8–10]. Other major processes that alter the power in a beam include laser backscatter and plasma absorption [11]. In other words, the power incident on the LEH from a particular laser beam may not be the power that beam delivers to the hohlraum wall.

In this article, we investigate the role certain laser-plasma interactions play on capsule flux symmetries. To that end, we develop a simplified model that captures some of the effects of laser plasma interactions on laser powers, which can then be fed into view factor calculations of capsule flux. The model, `lasertram`, takes NIF experimental laser powers and pointings and returns powers adjusted to account for various physical processes. These powers can be read directly into the view factor code VisRad [12] and used to calculate the radiation field inside of NIF hohlraums. In sum, the model marries the important laser plasma interaction processes to view factor calculations for quick estimates of capsule flux.

At present, `lasertram` contains various models to incorporate power fluctuations, crossed-beam energy transfer, laser backscatter and plasma absorption, which we describe briefly in Section II (additional details appear in the appendices). In Section III, we apply the new model to the problems of random laser power fluctuations and missing laser quads, proposing a scheme to limit the effects of dropping laser quads on capsule symmetry.

II. LASERTRAM: THE LASER TRANSFER MODEL

The view factor preprocessor, `lasertram`, adjusts NIF laser quad powers to mimic physical processes thought to be important in NIF experiments. It is written in `python` and can be run on a desktop computer in a few seconds. At present, `lasertram` can model the effects of as-delivered power fluctuations, crossed-beam energy transfer, laser backscatter and absorption. These processes are assumed to work sequentially; that is for a vector of initial laser quad powers $\vec{P}^0$, the final power delivered by those lasers to the hohlraum wall after laser-plasma interactions and hydrodynamics is given by:

$$\vec{P}^f = \mathcal{A} \cdot \mathcal{B} \cdot \mathcal{T} \cdot \mathcal{S} \cdot \vec{P}^0. \quad (1)$$

Each physical process is represented by a operator. The first operator, $\mathcal{S}$, represents a scaling of the initial powers. This is useful for studying the effects of as-delivered per-quad powers, such as from random experimental fluctuations. The next operator, $\mathcal{T}$, models crossed-beam energy

* peterson76@llnl.gov

transfer. Power losses due to backscatter and plasma absorption are represented by $\mathcal{B}$ and $\mathcal{A}$ respectively. Full details on the operators appear in the Appendices.

After applying these operators, the final powers $\vec{P}^f$ are written along with the beam orientations ("pointings") in a format that can be imported into the view factor code VisRad. Lasers in a quad are assumed to have the same power, but each beam has its own pointing. In its simplest operation with all operators equal to the identity matrix, `lasertram` is an expedient method to transfer experimentally delivered NIF powers and pointings into VisRad.

The goal of `lasertram` is to study the effects of different physical processes on laser power and radiation drive on NIF capsules. One advantage of applying these operators sequentially is the ability to study the trickle-down effects of different physical processes. As an example, an increase in as-delivered quad power can be spread to other quads through crossed-beam energy transfer. This method also allows one to compare the effects of different physical processes. Laser backscatter ($\mathcal{B}$) can be measured [13], but the power that heats up the plasma and sustains the hohlraum albedo ($\mathcal{A}$) is less certain.

The final power in quad i, P_i^f is related to its initial power P_i^0 by the absorption, backscatter, crossed-beam transfer and scale factors:

$$P_i^f = (1 - A_i)(1 - B_i)T_i S_i P_i^0. \quad (2)$$

Equation 2 represents the entire `lasertram` procedure. Quad i has its power scaled by a factor S_i. It gains or loses power via crossed-beam energy transfer, with an effective multiplier of T_i. Finally, it loses fractions B_i and A_i to backscatter and absorption before reaching the hohlraum wall.

In general, the final power delivered to the hohlraum wall will be less than delivered by the laser. As an example, consider a 23.5-degree beam, $k = 24$ (integer subscripts k represent the approximate polar angle of an entire cone; see Appendix A), which we will not manually scale ($S_k = S_{24} = 1$). The outer beams are often run to transfer energy to the inner beams, so $T_{24} \sim 1.7$. A typical amount of backscatter on inner quads is 30 percent, so $B_{24} \sim 0.3$. For an assumed albedo of 0.9 the inner beams must lose about 85 percent of their post-backscatter energy for view factor calculations to agree with radiation hydrodynamic simulations of hohlraum wall emission and radiation temperature (see Appendix B), so $A_{24} \sim 0.85$. Equation 2 says that the final power on the inner quad is only about 18 percent of its initial power. Typical numbers for outer quads ($T_k = 0.7$, $B_k = 0$, $A_k = 0.4$) calculate a total coupling efficiency of 42 percent, even without backscatter. The "missing" energy implied by $A_k < 1$ is not missing, but rather is tied up in the hohlraum plasma. In our calculations it is a parameter used to sustain an assumed hohlraum albedo.

III. IMPLICATIONS OF EXPERIMENTAL FLUCTUATIONS

We now apply `lasertram` to two experimentally relevant problems. The first concerns random power fluctuations across all quads; the second involves the loss of a single laser quad in its entirety. These two realities have the potential to impact capsule drive symmetry. In both cases crossed-beam energy transfer has a nonlinear effect, because in our saturated transport model (see Appendix A) the power transferred to quad i comes from the coupling of quad i to all other quads j in some interaction volume δz:

$$P_i(z + \delta z) = P_i(z) + \sum_j c_{i,j}(z)\sqrt{P_i(z)P_j(z)}. \quad (3)$$

If a quad is dropped, energy cannot be transferred to or from it. Additionally, the effect of cross-correlations between randomly fluctuating quads on power transfer is unknown. In this section, we use `lasertram` to address these questions.

Our test-bed is NIF shot N111215 at peak power (19.0 ns), which was a 1.45 MJ, 432 TW DT implosion. Informed by the calibration in Appendix B, we assume an albedo of 0.9 for the view factor calculations and set $B_{\rm in} = 0.3$, $B_{\rm out} = 0$, $A_{\rm in} = 0.85$ and $A_{\rm out} = 0.4$, where "in" and "out" represent values for all inner or outer cones. As mentioned in Appendix B, the backscatter values are representative of typical measurements, and the absorption values are such that the view factor calculated radiation temperatures and inner/outer power fraction on the hohlraum wall agrees with radiation hydrodynamic simulations. We will also use the one- dimensional crossed-beam transfer model, Eq. 3. Although N111215 had a "three-color" wavelength separation ($\lambda_{24} = \lambda_{45,50} + 6.6$ Å, $\lambda_{30} = \lambda_{45,50} + 8.1$ Å), we use the "two-color" matrix coefficients $c_{i,j}$ detailed in Appendix A that are valid for shot N110807 with $\Delta\lambda_{24} = \Delta\lambda_{30} = 5.5$ Å. The laser beams have as- fired orientations (pointings); we do not attempt to model beam bending [14].

The view factor model simulates a hohlraum with dimensions characteristic of the peak of the laser pulse. The three-dimensional model is built in VisRad [12] and consists of a cylindrical hohlraum and a capsule. The hohlraum has a radius of 0.2575 cm, a length of 0.9425 cm and an LEH radius of 0.1685 cm. The hohlraum radius is 0.03 cm less than the nominal pre-shot radius of 0.2875 cm to simulate the motion of the inner hohlraum wall by peak power. (Although in reality the wall motion is not uniform, and the hohlraum distorts more locally under the beam spots than elsewhere; to maintain cylindrical symmetry, we ignore this effect.) The hohlraum is made of 40 axial and 48 azimuthal grid points, and the end disks have 12 radial grid points. The capsule has a radius of 0.08864 cm, which is 80 percent of the pre-shot 0.1108 cm, to simulate conditions at the early stages of compression. The spherical capsule has 50 polar and 50

azimuthal grid points and an albedo of 0.15. These resolutions have been tested for convergence in resolving the incident capsule flux up through the mode l=4 spherical harmonics.

A. Crossed-Beam Transfer and Power Fluctuations

To investigate the role crossed-beam energy transfer could have on random laser power fluctuations, we simulate via Monte Carlo sampling random variations in laser quad powers about the mean N111215 peak power values. We assume Gaussian distributions characterized by an initial standard deviation σ_i^0 for each quad i, so that S_i is sampled from a distribution around 1. Then, we run each quad through the beam-coupling crossed-beam energy transfer model and collect statistical info on the distribution of post-transfer quad powers.

Quad i has a pre- and post-transfer fluctuation level characterized by Δ_i^0 and Δ_i^f. These levels are defined as the standard deviation of the ensemble of powers normalized to the ensemble's mean:

$$\Delta_i^0 = \sigma_i^0/\bar{P}_i^0, \tag{4}$$

$$\Delta_i^f = \sigma_i^0/\bar{P}_i^f. \tag{5}$$

The pre- and post-transfer average quad powers are $\bar{P}_i^0$ and $\bar{P}_i^f$, respectively. Together, they describe the quad's average power transfer multiplier $T_i \doteq \bar{P}_i^f/\bar{P}_i^0$.

We let Δ_i^0 be the same for every quad in a simulation ($\Delta_i^0 = \Delta^0$) and let $\Delta^0 = [1, 2, \ldots 5]$ percent. Each of these 5 simulations consists of an ensemble of 5000 samples.

Figure 1 plots the post-transfer fluctuation amplitude Δ_i^f, as calculated from the 5000-point ensemble for each quad i in the five different simulations. Every quad obeys the same rule, which relates the post-transfer fluctuation amplitude to the pre-transfer fluctuation level:

$$\Delta_i^f = \Delta^0/\sqrt{T_i}. \tag{6}$$

Equation 6 quantifies how beam-to-beam coupling during crossed-beam energy transfer alters a laser's statistical level of fluctuations. In particular, a quad's response depends on the amount of energy it gains or loses during the energy transfer process. A consequence of Eq. 6 is that as quads gain energy during transfer, their relative fluctuation level actually decreases. The reverse is true for quads that lose power during transfer.

Some algebraic consequences follow from Eq. 6. Firstly, the absolute magnitude of the post-transfer fluctuation level increases with the amount of power transfer:

$$\sigma_i^f = \sigma^0\sqrt{T_i}. \tag{7}$$

In other words, crossed-beam transfer causes both the mean and variance of a laser quad's power to be multiplied by the quad's average transfer coefficient T_i:

$$\left(\sigma_i^f\right)^2 = \left(\sigma^0\right)^2 T_i, \tag{8}$$

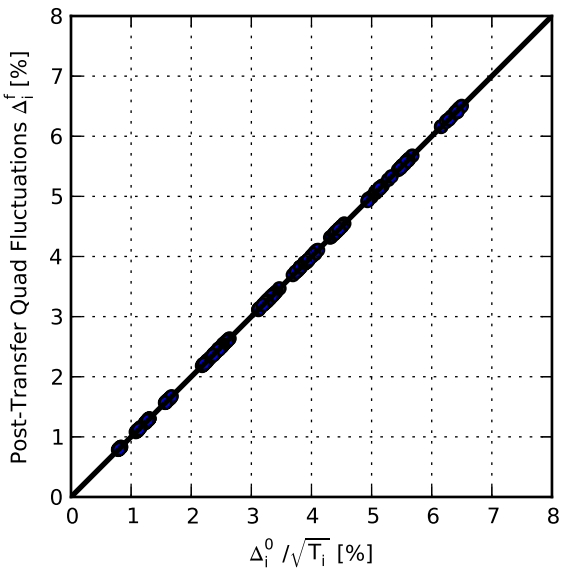

FIG. 1. Post-transfer fluctuation amplitudes for each quad i, Δ_i^f, plotted against $\Delta_i^0/\sqrt{T_i}$, where Δ_i^0 is the quad's pre-transfer fluctuation amplitude and T_i is the average power multiplier on quad i due to energy transfer.

$$\bar{P}_i^f = \bar{P}_i^0 T_i. \tag{9}$$

Using these rules and examining different sub-sets of quads can inform how groups of cones and the entire set of laser quads vary. Each cone ensemble follows a rule that depends on the average cone transfer multiplier T_{cone}:

$$\Delta_{\text{cone}}^f = \Delta_{\text{cone}}^0/\sqrt{T_{\text{cone}}}, \tag{10}$$

so that the inner cones' fluctuation levels decrease and the outer cones' fluctuation levels increase. Using the same numbers as in Table II at 19 ns, $\Delta_{30}^f/\Delta_{30}^0 = 0.79$, but $\Delta_{45}^f/\Delta_{45}^0 = 1.27$. As an example, if all quads enter the hohlraum with a 5 percent root-mean-square (rms) fluctuation level, crossed-beam transfer will shrink the 30-degree quads' distribution to about 4 percent, but increase the 45-degree distribution to 6.4 percent.

The total fluctuation amplitude, as measured by the ensemble of all laser quads can be calculated from the average cone transfer coefficients:

$$\Delta^f = \Delta^0 \sum_{\text{cones}} \frac{f_{\text{cone}}}{\sqrt{T_{\text{cone}}}}, \tag{11}$$

where f_{cone} is the fractional number of quads in a given cone, Δ^f is the total fluctuation amplitude of all quads after transfer and Δ^0 is the total fluctuation amplitude of all quads before transfer. In particular, since one sixth of the quads are 23.5-degree beams, (assuming up-down symmetry), one sixth are 30-degree beams, one third are

44.5-degree beams and one third are 50-degree beams, the total post-transfer fluctuation level is:

$$\Delta^f = \Delta^0 \left(\frac{1}{6\sqrt{T_{24}}} + \frac{1}{6\sqrt{T_{30}}} + \frac{1}{3\sqrt{T_{45}}} + \frac{1}{3\sqrt{T_{50}}} \right), \quad (12)$$

where T_{24}, T_{30}, T_{45} and T_{50} are the average transfer coefficients for each of the cones. As an example, consider the transfer coefficients as in Table II at 19.0 ns (1.49, 1.61, 0.62 and 0.82 for the 23.5-, 30-, 44.5-, and 50-degree beams respectively, corresponding to average values calculated for NIF shot N110807 at a wavelength separation $\Delta\lambda = 5.5$ Å). Equation 12 calculates that $\Delta^f/\Delta^0 = 1.16$. So if before transfer the laser beams were sampled from within a 3 percent rms distribution (which is the NIF Rev5 requirement during the peak of the laser power [4]), after transfer they have a 3.5 percent rms distribution. As shown above, individual cone distributions can vary by much more, so that although the inner quads have a more narrow distribution after transfer, the more numerous outer quads weight the total ensemble towards a wider distribution after transfer than before.

Since we assume that the coupling coefficients between quads, $c_{i,j}$, are constant, this model only considers the alteration of fluctuation levels due to power fluctuations. Certainly, if the local plasma conditions vary, which they likely will for large amplitude fluctuations, $c_{i,j}$ may change, and the $1/\sqrt{T}$ scaling may not hold. However, this model does allow for predictions at different conditions, if the cone transfer coefficients are known. For instance, if the laser wavelength separation $\Delta\lambda$ changes and modifies T_{cone}, Δ^f_{cone} should still follow Eq. 11.

B. Dropping a Quad

Occasionally a NIF shot will operate without one or more laser quads participating in a shot. When this occurs, the "dropped quad" does not fire. Consequently, it can neither give nor receive energy from crossed-beam energy transfer. Therefore, dropping a quad changes the incident capsule flux through two mechanisms: the missing beam spot on the wall (where the dropped quad would have deposited energy) and the altered energy in the quads that would have transferred energy with the dropped quad, if it were not dropped. Since the inner quads primarily gain power during transfer, and the outer quads primarily lose power during transfer, dropping outer and inner quads are expected to alter the final symmetry differently.

Figure 2 shows the change in incident capsule flux from dropping quad 25T, which is a 44.5 degree outer quad, by setting $S_{25\text{T}} = 0$ in `lasertram`. The difference is measured relative to the background case, in which no quads are dropped. The flux over the entire capsule is lower, due to the missing energy in the hohlraum: the mean flux drive with the dropped quad is 97.5 percent of

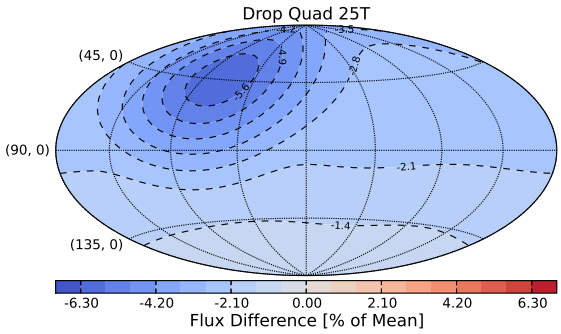

FIG. 2. The change in incident capsule flux when dropping quad 25T as measured relative to the background case. 25T is a 44.5 degree (outer) quad.

the baseline case. Additionally a large flux deficit lies on the capsule directly beneath 25T. The magnitude of this deficit is approximately 6 percent, but since the flux over the whole capsule is lower, the peak-to-valley difference is approximately 4.5 percent. Dropping an outer quad creates a localized flux defect on the capsule and lowers the overall capsule drive.

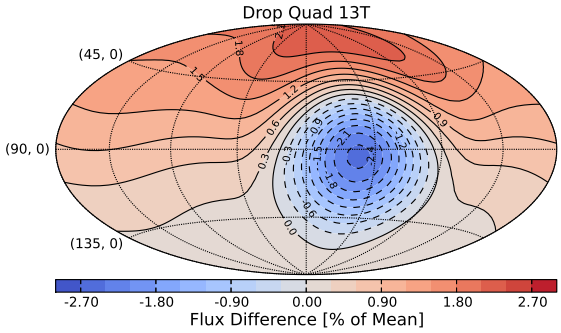

FIG. 3. The change in incident capsule flux when dropping quad 13T as measured relative to the background case. 13T is a 30 degree (inner) quad.

The effects of a dropped inner quad are different. Figure 3 show the change in capsule incident flux from dropping quad 13T, a 30 degree quad. Like the dropped outer quad case, a localized flux deficit appears on the capsule beneath the dropped quad's beam spot location on the hohlraum wall. It is not as large as the hole from dropping 25T (approximately 2.5 percent). However, other areas of the capsule are driven harder when dropping an inner quad. In particular, a hot spot appears near the north pole, due to an increased amount of flux in the outer quads that give power to 13T during crossed-beam energy transfer. Since 13T was dropped, this extra energy is stuck in those outer quads. The peak amplitude of this hotspot is slightly above 2 percent, but more diffuse than the localized cold spot beneath 13T, so that

the total peak-to-valley flux perturbation is comparable to that from dropping the outer quad.

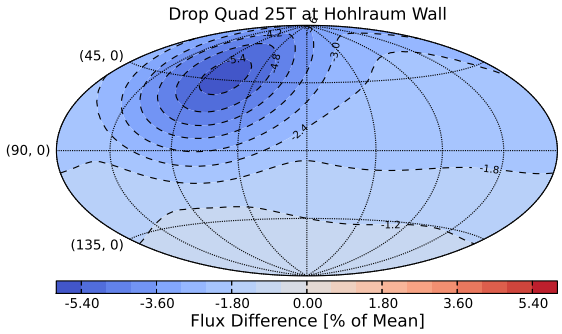

FIG. 4. The change in incident capsule flux when dropping quad 25T at the hohlraum wall, after crossed-beam energy transfer.

To illustrate the effects of nonlinear coupling between beams during crossed-beam energy transfer, Figures 4 and 5 show the change in capsule flux relative to the baseline case when removing the energy in 25T and 13T at the hohlraum wall by zeroing out the laser beams in VisRad. As such, Figures 4 and 5 show only the geometrical viewfactor effects of missing a quad. The flux deficit from dropping 25T at the hohlraum wall is very similar to the case when dropping the quad before crossed-beam energy transfer, although the mean drive is slightly higher when crossed-beam effects are not included (97.8 percent versus 97.5 percent). This is because when including energy transfer, 25T transfers energy to inner quads, which then lose a fraction of this energy via backscatter and impaired propagation. But in general, including crossed-beam effects when calculating the flux deficit from dropping an outer quad has a small effect on the change in capsule drive.

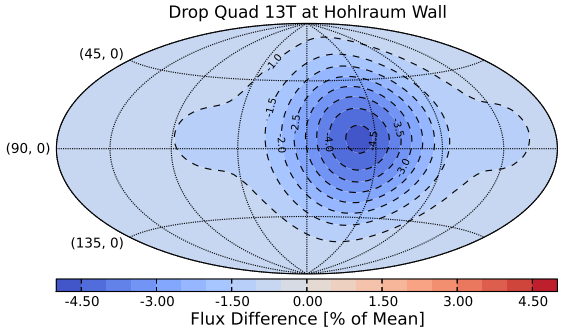

FIG. 5. The change in incident capsule flux when dropping quad 13T at the hohlraum wall, after crossed-beam energy transfer.

However, including crossed-beam coupling is much more important when calculating the flux due to dropping an inner quad. Figure 5 shows the change in capsule incident flux when removing 13T at the wall. This purely geometrical case shows a localized flux deficit beneath 13T of about 4.5 percent in peak amplitude. However, unlike Figure 3, which includes the effects of crossed-beam energy transfer, no capsule hot spots appear; the drive on the capsule is lower everywhere. The salient point is that when dropping an inner quad, both a hot spot and a cold spot appear on the capsule, due to the nonlinear coupling between quads during crossed-beam energy transfer. The peak-to-valley amplitude of the capsule flux is about 4.5 percent in both cases, but it is distributed differently on the capsule. And the mean drive when including energy transfer is higher (100.6 percent versus 98.7 percent).

It is interesting to note that dropping an inner quad actually *increases* the mean drive on the capsule, because the energy trapped in the outer quads is not depleted as much by backscatter and absorption as it propagates to the wall as it would have had it been transferred to the missing inner quad. Dropping an inner quad alters the shape of the incident drive, in this case the capsule is perturbed along the axial and equatorial directions. Not including crossed-beam energy transfer would perturb the drive only in the equatorial direction.

Dropping a quad creates a drive perturbation of about 4.5 percent in peak-to-valley amplitude. When dropping an outer quad, this is a localized cold spot on the capsule beneath the missing beams. When dropping an inner quad, the perturbation appears not only as a cold spot beneath the missing beams, but also as a hot spot beneath the beams that would have transferred energy to the missing beam.

C. Compensating for a Dropped Quad

On occasion quads will be intentionally redirected away from the hohlraum, for instance onto a backlighter foil for radiographic imaging. Recently, experiments have been fielded to use these techniques to image the in-flight capsule shell [15, 16], the goal being to quantify and correct shell distortions.

A concern, however, is that the asymmetries introduced by the missing backlighter beams would compromise the measurement by altering the radiation field inside the hohlraum.

Figure 6a shows the change in incident capsule flux as calculated by view factors from dropping the backlighter quads in the axial 2D Convergent Ablator (ConA) Experiment [16], which uses radiography to image the imploding shell looking down the hohlraum axis from the north pole. Uncompensated, the backlighter beams each create a flux hole on the capsule southern hemisphere of roughly 10%. View factor calculations (Figure 6b) suggest that if the incident laser power at the hohlraum wall can be increased by 20% in the 8 quads nearest to the flux holes and by 10% in all other lower hemisphere outer quads, the capsule flux perturbation can be reduced sig-

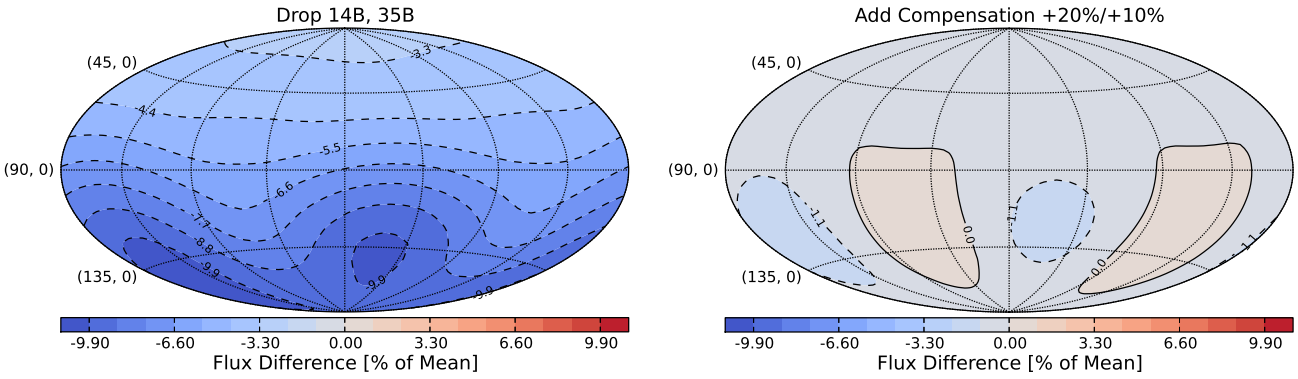

(a) Uncompensated backlighter quads

(b) Compensated backlighter quads

FIG. 6. (a) The change in incident capsule flux when dropping the outer beam backlighter quads for the axial 2D conA experiment at the wall. (b) The effect of increasing the 4 quads nearest to backlighter by 20% and increasing all other lower outer quads by 10%.

nificantly, down to roughly one percent. More specifically, the scheme is to locate where on the hohlraum wall a missing backlighter quad would have struck. The power in the two quads on each side of that hole (4 total) are increased at the wall by 20%. The same is done for the other backlighter quad. All other lower hemisphere outer quads are increased by 10% to help maintain the overall up-down flux symmetry.

For the axial 2D ConA experiment, the backlighter quads are Q14B and Q35B. Both are outer quads in the lower hemisphere with a polar angle of 135.5 degrees. The +20% "nearest neighbors" are Q11B, Q12B, Q13B, Q22B, Q32B, Q34B, Q36B and Q45B. The remaining +10% outer quads are Q23B, Q25B, Q26B, Q41B, Q43B and Q46B. The goal is to increase the flux delivered by these quads to the hohlraum wall by the specified values.

However, crossed-beam energy transfer complicates the process. In our model, the power in a quad after transfer P_i^f depends on the power before transfer P_i^0:

$$P_i^f = P_i^0 + \sum_j c_{i,j}\sqrt{P_i^0 P_j^0}. \tag{13}$$

Consider increasing P_i^0 to a new value $\hat{P}_i^0$ by some small amount ϵ, $\hat{P}_i^0 \doteq (1+\epsilon)P_i^0$. Using T_i as the unperturbed transfer coefficient $T_i \doteq P_i^f/P_i^0$, Eq. 13 for $\hat{P}_i^0$, and a little algebra shows how ϵ alters the post-transfer power:

$$\frac{\hat{P}_i^f}{P_i^f} = \frac{1+\epsilon-\sqrt{1+\epsilon}}{T_i} + \sqrt{1+\epsilon}. \tag{14}$$

In essence, Eq. 14, shows that for quads undergoing transfer, the post-transfer power increase will not equal the pre-transfer power increase. As an example, consider a 30-degree quad with $T = 1.6$ (the average value for $\Delta\lambda = 5.5$ Å). If $\epsilon = 0.1$, Eq. 14 says that $\hat{P}^f = 1.08P^f$. That is, increasing the pre-transfer power by 10% yields a post-transfer power increase of only 8%.

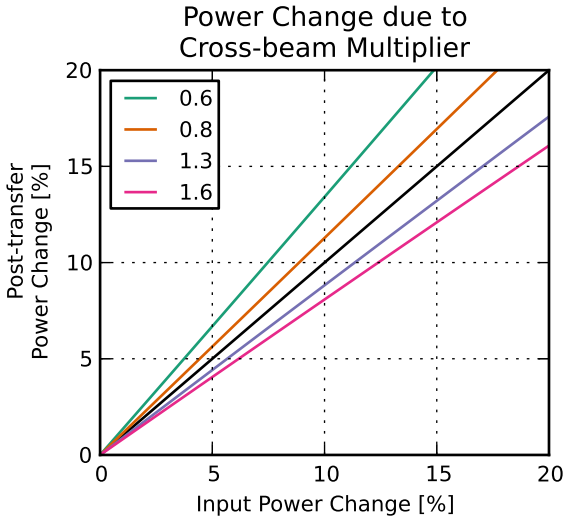

FIG. 7. The change in quad laser power after cross-beam energy transfer for different transfer coefficients.

Figure 7 shows this effect for a range of input power increases and for typical transfer coefficients. Outer quads, whose transfer coefficient is less than one, see an increase in post-transfer power relative to pre-transfer power. Specifically, to increase the power after transfer by 20% in 44.5-degree quads, with a transfer coefficient of approximately 0.6, requires a pre-transfer increase of only about 15%. 50-degree quads with a transfer coefficient of 0.8 need an additional 17.5% power. This effect is beneficial, because it can relax the conditions on

the laser to achieve a desired outer-beam flux increase at the wall. (Incidentally, it also implies that compensation with inner beams is likely to be less effective.)

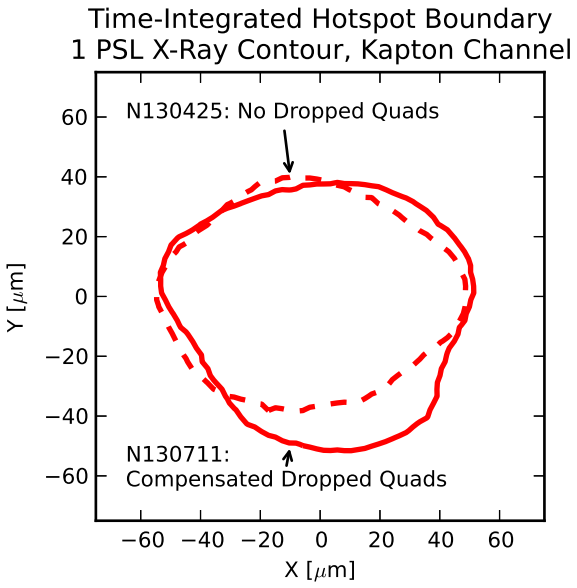

FIG. 8. Equatorial time-integrated self-emission contour for NIF shots N130711 (solid) and N130425 (dashed). The 1.0 PSL x-ray contour corresponds to 17.3% of the maximum brightness for the Kapton channel for N130711, approximately outlining the central hotspot. The view is on the equator, along angle $(\phi, \theta) = (90, 78)$. As compared to N130425, N130711 dropped two lower hemisphere quads for backlighting, but employed the compensation scheme developed in the main text.

Accomplishing the backlighter compensation scheme in Figure 6b requires a consideration of this effect. To increase the "nearest neighbor" 44.5(50)-degree quads by 20% at the hohlraum wall requires a laser power increase of 17.5(15)%. Similarly, the non-nearest neighbor 44.5(50)-degree quads need an additional 7.5(9)%. The axial 2D ConA compensation scheme, therefore, involves four families of quads: {Q23B, Q41B, Q46B}, {Q25B, Q43B}, {Q11B, Q13B, Q34B, Q36B}, and {Q12B, Q22B, Q32B, Q45B}, which are requested to have laser power increases of 7.5, 9, 15 and 17.5%, respectively.

This backlighter compensation method was fielded on the axial 2D ConA experiment, NIF shot N130711 [16]. Neither the in-flight radiograph nor the polar self-emission images show evidence of localized distortions from the missing backlighter quads; however, the equatorial hot-spot self-emission does show distortions in the lower hemisphere, as compared to the symcap companion shot, N130425, which did not drop any quads for backlighting. Figure 8 compares the 1.0 photostimulated luminescence (PSL) x-ray self-emission brightness levels as measured by the time-integrated Kapton channel for the two shots. This brightness level corresponds to 17.3% of the maximum value recorded for N130711 and roughly outlines the central hotspot. The two shots have very similar shapes in the upper hemisphere, but the shot with the compensated dropped quads shows a distortion in the lower hemisphere. This is to be expected from the flux maps in Fig. 6b, which show two localized drive deficits in the lower hemisphere of the capsule. N130711 shows a hotspot distortion of around 30 percent, as compared to the unperturbed case. Dividing this distortion by the hotspot convergence ratio (27.5) gives an estimated flux perturbation of 1.1 percent, consistent with the predicted flux map for the compensation scheme in Fig. 6b.

Although NIF quads must be occasionally excluded from a shot, it is possible to spatially compensate for their absence, ameliorating their deleterious effects on capsule shape. Crossed-beam energy transfer can enhance the effects of outer-beam power increases, making their use in compensation schemes less energetically taxing.

IV. DISCUSSION AND CONCLUSIONS

Laser-plasma interactions alter the power in a NIF laser beam as it travels from the hohlraum laser entrance hole to the hohlraum wall. The effects of these LPI processes on capsule flux in the presence of experimental laser fluctuations are largely unexplored. To that end, we have built a code `lasertram` to model crossed-beam energy transfer, backscatter and absorption and have applied the model to two experimentally relevant situations: the dropping of a laser quad and random power fluctuations.

When an outer quad is missing from an experiment, the flux incident on the capsule is perturbed locally underneath the missing beam spot on the hohlraum wall. This perturbation appears as approximately a 4.5 percent "cold spot" on the capsule, and the effect is mostly geometrical, since including quad-to-quad crossed-beam energy transfer doesn't significantly alter this picture. However, energy transfer plays a more important role when dropping an inner quad, since the energy that would have been transferred to the missing quad is trapped in other quads. The result is the existence of not only a localized cold spot, but also a hot spot under the quads with the trapped energy. Each spot has a magnitude of approximately 2-2.5 percent, so that the peak-to-valley flux difference is comparable to dropping an outer quad.

In either case, the perturbation on the capsule is likely enough to impact the experiment, because radiation hydrodynamic simulations of capsules have shown significant distortion and performance degradation under flux asymmetries of a few percent [4, 17–19]. However, we have shown that it is possible to spatially compensate for missing quads, and that crossed-beam energy transfer enhances the effectiveness of outer-beam quads in this regard.

Crossed-beam energy transfer also alters the statisti-

cal properties of uncorrelated laser power fluctuations in a manner that depends on the mean amount of energy transferred. If all laser beams enter the hohlraum with the same statistical distribution, they will strike the hohlraum wall with a different distribution. Quads that gain energy during transfer will have a narrow distribution, and quads that lose energy will have a broader distribution. In other words, outer beams are expected to strike the hohlraum wall with more random power variation than do inner quads. This process could have experimental implications, since random laser power requirements assume that the distribution of laser energy does not change while it propagates to the hohlraum wall. Future work will involve determining the effect of these laser fluctuations on the incident capsule flux.

Appendix A: Details on the `lasertram` Operators

Herein, we describe details on the different options for the operators in `lasertram` that translate a vector of initial laser powers into a vector of final powers.

The scaling operator $\mathcal{S}$ models as-delivered powered fluctuations. It is a diagonal matrix, the components of which can be specified on a per-quad or per-cone basis. (A cone is a group of beams with the same incident angle with respect to the hohlraum axis. NIF has 8 distinct cones.) The operator $\mathcal{S}$ effectively multiplies the LEH power by a given factor and can be used to study the effects of as-delivered drive power.

A few different models exist in `lasertram` to represent the crossed-beam transfer operator, $\mathcal{T}$. The simplest method involves cone-specified multiplicative factors. Namely one can specify a scale factor T_k, where the integer $k \in \{24,\ 30,\ 45,\ 50,\ 130,\ 135,\ 150,\ 156\}$ represents the approximate polar angle of the laser quad. "Inner" beams have k of 24, 30, 150 or 156. The other angles form the "outer" beams. Typical values of T_k range from $1.6 - 1.8$ for the inner cones and $0.6 - 0.8$ for the outer cones. In other words, NIF generally operates within a regime whereby energy is transferred from the outer cones to the inner cones. `lasertram` can also specify T_i on an individual quad basis.

In lieu of manually setting the amplification factor of all cones or beams, one can specify only inner cone factors and reduce the outer cones to conserve energy. Let P_k represent the total power in all of the quads in cone k before applying crossed-beam transfer and let P_{out} be the total power in the outer cones. Given T_{24} and T_{30}, we calculate T_{out} to conserve energy. Specifically, the total power prior to transfer

$$P_{\text{out}} + P_{24} + P_{30} + P_{150} + P_{156}, \tag{A1}$$

should be equal to the total after transfer:

$$T_{\text{out}} P_{\text{out}} + T_{24}\left(P_{24} + P_{156}\right) + T_{30}\left(P_{30} + P_{150}\right). \tag{A2}$$

For simplicity, we have assumed up-down symmetry on the transfer coefficients. The transfer coefficient on the outer cones can be determined by equating Eq. A1 and Eq. A2:

$$T_{\text{out}} = 1 + \frac{\left(P_{24} + P_{156}\right)\left(1 - T_{24}\right) + \left(P_{30} + P_{150}\right)\left(1 - T_{30}\right)}{P_{\text{out}}}. \tag{A3}$$

Eq. A3 is referred to as the energy-conserving inner amplification method.

The final method for crossed-beam energy transfer incorporated into `lasertram` is a one-dimensional integration model of quad-to-quad interactions. Quad transfers are presently calculated on NIF by propagating individual quads through the three-dimensional LEH and determining each quad's interaction with the other 23 quads in its hemisphere. The intensity of each quad changes as it propagates through this volume and interacts with the other quads and the background plasma. As quad i moves a distance δz along the hohlraum axis, its intensity I_i changes from interactions with the other j quads:

$$I_i(x, y, z + \delta z) = I_i(x, y, z) + C \sum_{j=1}^{24} K_{i,j}(x, y, z) \sqrt{I_i(x, y, z) I_j(x, y, z)}. \tag{A4}$$

The coupling matrix $K_{i,j}$ depends upon the plasma properties at the LEH and the relative geometries of the laser quads. The square root dependence approximates saturated energy transfer, valid at peak laser power. Integrating over x and y and rewriting in terms of laser quad powers yields an equation for saturated power transfer:

$$P_i(z + \delta z) = P_i(z) + \sum_{j=1}^{24} c_{i,j}(z) \sqrt{P_i(z) P_j(z)}. \tag{A5}$$

The coupling coefficients $c_{i,j}$ can be extracted from a full crossed-beam calculation by looking at the change in each quad's power during integration along the hohlraum axis, $\Delta P_i(z)$:

$$c_{i,j}(z) = \frac{\Delta P_i(z)}{\sqrt{P_i(z) P_j(z)}}. \tag{A6}$$

This method effectively decouples the quad powers from the crossed-beam calculation. For a given set of $c_{i,j}$ and

the same input powers $P_i(z=0)$, both the full crossed-beam calculation and the reduced model, Eq. A5, should calculate identical transfer coefficients. The implementation in `lasertram` takes as input a set of $c_{i,j}$ (as extracted from a full crossed-beam calculation) and scaled powers $(\mathcal{S}\cdot\vec{P}^0)$. To be explicit, the transfer coefficient for a quad i can be written then as:

$$T_i = \frac{P_i(z=N_z\delta z)}{S_i P_i^0}. \tag{A7}$$

The final value of z, $N_z\delta_z$, is calculated via numerical integration. In practice, $c_{i,j}$ is a three-dimensional matrix extracted from the full crossed-beam transfer code: $c_{i,j,k}$ with dimensions $[24, 24, N_z]$. With δz assumed to be unity, the numerical integration becomes a sum along the third dimension.

Since full crossed-beam calculations only include laser quads in the upper hemisphere ($i = 1\ldots24$), we calculate the lower hemisphere's power by mapping $c_{i,j}$ from an upper quad to a corresponding lower quad with the same relative geometry, but calculate the lower quad's transfer using its input powers. This allows for upper and lower quads to have potentially different transfer coefficients due to variations in quad powers, but the plasma conditions at the LEH and the geometric coupling factors (which together determine $c_{i,j}$) are assumed up-down symmetric. As an example where this may be useful, we consider the case of a dropped quad in the upper hemisphere, that is $P_i(z=0)=0$. No quads will transfer power with quad i; however, quads may continue to transfer power with quad i's mirror in the lower hemisphere, i', because $P_{i'}\neq 0$, and we assume $c_{i,j} = c_{i',j'}$.

TABLE I. Cone-averaged crossed-beam energy transfer coefficients for shot N110807 at 19.5 ns, as determined by the full three-dimensional calculation (with $\Delta\lambda = 5.5$ Å) and by the reduced `lasertram` model.

	Transfer Coefficient		
Cone Angle	Full Calculation	Reduced Model	% Error
23.5 degrees	1.5087	1.5100	0.09
30 degrees	1.6178	1.6220	0.26
44.5 degrees	0.6230	0.6224	0.10
50 degrees	0.8222	0.8204	0.22

To summarize, the one-dimensional crossed-beam transfer calculation isolates the laser power dependency from a crossed-beam energy transfer calculation. Other effects are assumed to be captured in the coefficients $c_{i,j}$, which are extracted from a higher-fidelity crossed-beam transfer calculation. As such, the reduced model is designed to agree with the full model when both are run with the same conditions that generated the coupling coefficients. This fidelity is displayed in Table I, which compares the cone-averaged transfer coefficients for NIF shot N110807 at 19.5 ns as determined by a full three-dimensional calculation (corresponding to an inner-outer wavelength separation $\Delta\lambda = 5.5$) and by the reduced one-dimensional model, using $c_{i,j}$ as extracted from the full calculation.

The backscatter and absorption operators, respectively $\mathcal{B}$ and $\mathcal{A}$, are diagonal matrices that scale the post-crossed-beam quad powers. One specifies as input the fractional amount lost in each quad for these processes, using either a uniform factor for all quads or different factors for each cone. Unlike the crossed-beam scale factors T_i, which represent power multipliers, the backscatter and absorption factors B_i and A_i represent loss fractions. Each quad i is then multiplied by the factor $(1-B_i)$ for backscatter and $(1-A_i)$ for absorption. It should be noted that the energy lost by absorption represents the energy required to ionize the hohlraum gas and support its albedo. Full radiation-hydrodynamic simulations conserve this energy, but it does not appear as radiation energy incident on the hohlraum that can re-radiate in a directed fashion toward the capsule. Instead, this energy should be viewed as a volumetric source within the hohlraum. Including this volumetric source alters the effective albedo of the hohlraum but does not appreciably change symmetry. For the view factor calculations, we will therefore consider the energy lost and pick an appropriate albedo.

Appendix B: Calibrating the Model

The strength of the `lasertram` model is in its flexibility: one can adjust the laser powers in a variety of methods. However, this is not without its limitations, because the applicability of the model to NIF experiments relies on a careful choice of these parameters. Here, we find a set of input parameters that gives good agreement with a three-dimensional radiation hydrodynamics simulation of the hohlraum done with HYDRA [20].

To calibrate the model, we will adjust the crossed-beam, backscatter and absorption parameters so that a view factor calculation based on those parameters matches calculations from a fully three-dimensional radiation hydrodynamic simulation. We will tune our model to NIF shot N110608 at three time points: 1.0 ns, 1.5 ns and 19 ns. These times correspond to the peak laser power in the first picket, the peak radiation temperature in the picket and the peak of the laser pulse. Specifically, we aim to match the total power and fraction of power in the inner cones after crossed-beam transfer and backscatter, as well as the radiation temperature and wall emission ratio. Crossed-beam transfer and backscatter settings (T_k and B_k) tune the first two parameters, without the need to run a view factor calculation. The last two, however, require a view factor calculation with an assumed albedo and absorption losses. Since there are two post-backscatter parameters to match, we will limit ourselves to two adjustable absorption coefficients: one for

the inner beams, and one for the outer beams. That is, we tune $A_{\rm in}$ and $A_{\rm out}$, with $A_{\rm in} = A_{24} = A_{30} = A_{156} = A_{150}$ and $A_{\rm out} = A_{45} = A_{50} = A_{130} = A_{135}$. Our view factor calculations are done with VisRad, assuming an albedo of 0.5 for $t = 1.0,\ 1.5$ ns and 0.9 for $t = 19$ ns.

To make the problem more tractable, we make some experimentally motivated assumptions during the different time points. At 1.0 and 1.5 ns we assume no backscatter losses and adjust the inner cone transfer multipliers (using the energy conserving method of Eq. A3 for the outer cones) to match the post-backscatter cone fraction. At 19.0 ns, we calculate crossed-beam transfer with the one-dimensional model of Eq. A7, and adjust the backscatter on the inner and outer cones to match the total power and inner cone fraction. By assuming a backscatter model in the picket and a crossed-beam model in the peak, we restrict the number of adjustable parameters to match the number of HYDRA-calculated observables.

Tables II and III respectively show the calibrated `lasertram` settings and measured observables from the combination `lasertram`/Visrad view factor calculation using those settings. Table III also shows HYDRA values for those observables and demonstrates that all four observables (the post-backscatter laser power, the post-backscatter inner cone fraction, the wall emission cone fraction and the radiation temperature) lie within the uncertainties of the HYDRA measurement.

The set of calibrated coefficients in Table II is not unique; a number of other possibilities for crossed-beam, backscatter and absorption exist that will give the same match to HYDRA. In other words, the view factor calculation only needs the same amount of power in the inner and outer cones to match the radiation temperature and wall emission cone fraction. A set of `lasertram` parameters with the same total coupling to the wall (that is the ratio of P^f to P^0) as those of Table II will match HYDRA just as well (because the input powers into the view factor calculation will be identical). For instance, one can accommodate the ansatz that at peak power the outer cones experience no backscatter losses and the inner cones lose 30 percent by maintaining $(1-B_k)(1-A_k)$ a constant. The tuned values in Table II show this constant to be $(1-0.25)(1-0.85) = 0.1125$ for the inner cones and 0.5775 for the outer cones. Asserting that $B_{\rm in} = 0.3$ and $B_{\rm out} = 0$ requires setting $A_{\rm in} = 0.84$ and $A_{\rm out} = 0.42$. This backscatter ansatz is in agreement with measurements of typical peak power backscatter losses on NIF [21]. As such, we can say that only about 15 percent of the post-backscatter energy makes it to the hohlraum wall for the inner beams. For the outer beams, this is closer to 60 percent. The remainder goes into heating the hohlraum plasma and supporting the wall's albedo.

ACKNOWLEDGMENTS

The authors would like to thank L. Suter, O. Jones and B. Kirkwood for useful discussions, J. Milovich for providing the HYDRA data, and N. Izumi for the NIF x-ray data. This work was performed under the auspices of the U.S. Department of Energy by Lawrence Livermore National Laboratory under Contract DE-AC52-07NA27344.

[1] G. H. Miller, E. I. Moses, and C. R. Wuest, Optical Engineering **43**, 2841 (2004).
[2] J. D. Lindl, Physics of Plasmas **2**, 3933 (1995).
[3] J. D. Lindl, P. Amendt, R. L. Berger, S. G. Glendinning, S. H. Glenzer, S. W. Haan, R. L. Kauffman, O. L. Landen, and L. J. Suter, Physics of Plasmas **11**, 339 (2004).
[4] S. W. Haan, J. D. Lindl, D. A. Callahan, D. S. Clark, J. D. Salmonson, B. A. Hammel, L. J. Atherton, R. C. Cook, M. J. Edwards, S. Glenzer, A. V. Hamza, S. P. Hatchett, M. C. Herrmann, D. E. Hinkel, D. D. Ho, H. Huang, O. S. Jones, J. Kline, G. Kyrala, O. L. Landen, B. J. MacGowan, M. M. Marinak, D. D. Meyerhofer, J. L. Milovich, K. A. Moreno, E. I. Moses, D. H. Munro, A. Nikroo, R. E. Olson, K. Peterson, S. M. Pollaine, J. E. Ralph, H. F. Robey, B. K. Spears, P. T. Springer, L. J. Suter, C. A. Thomas, R. P. Town, R. Vesey, S. V. Weber, H. L. Wilkens, and D. C. Wilson, Physics of Plasmas **18**, 051001 (2011).
[5] R. P. J. Town, D. K. Bradley, A. Kritcher, O. S. Jones, J. R. Rygg, R. Tommasini, *et al.*, Phys. Plasmas (accepted 2014).
[6] W. L. Kruer, Phys. Plasmas **3**, 382 (1996).
[7] V. V. Eliseev, Phys. Plasmas **3**, 2215 (1996).
[8] P. Michel, Phys. Rev. Lett. **102**, 025004 (2009).
[9] P. Michel, Phys. Plasmas **17**, 056305 (2010).
[10] J. D. Moody, P. Michel, L. Divol, R. L. Berger, E. Bond, D. K. Bradley, D. A. Callahan, E. L. Dewald, S. Dixit, M. J. Edwards, S. Glenn, A. Hamza, C. Haynam, D. E. Hinkel, N. Izumi, O. Jones, J. D. Kilkenny, R. K. Kirkwood, J. L. Kline, W. L. Kruer, G. A. Kyrala, O. L. Landen, S. LePape, J. D. Lindl, B. J. MacGowan, N. B. Meezan, A. Nikroo, M. D. Rosen, M. B. Schneider, D. J. Strozzi, L. J. Suter, C. A. Thomas, R. P. J. Town, K. Widmann, E. A. Williams, L. J. Atherton, S. H. Glenzer, and E. I. Moses, Nat Phys **8**, 344 (2012).
[11] W. L. Kruer, Phys. Plasmas **7**, 2270 (2000).
[12] J. MacFarlane, Journal of Quantitative Spectroscopy and Radiative Transfer **81**, 287 (2003).
[13] J. D. Moody, Rev. Sci. Instrum. **81**, 10D921 (2010).
[14] Beam bending could in principle be modeled outside of `lasertram` by altering the pointings in the view factor code. Since beam bending can be thought as cross-beam transfer between different parts of a quad due to the nozzle-like LEH plasma flow, the most extreme bending could be half the f-number of a quad, which corresponds to adding 3.7 degrees to each quad trajectory. View factor calculations with this case altered the ratio of the second Legendre mode to the mean capsule flux by 2 percent $[\Delta(P_2/P_0) = 2\%]$; higher modes are affected less due to hohlraum smoothing.

TABLE II. Best-calibrated settings for `lasertram` at different time points.

Time	Tuned `lasertram` Setting							
	$T_{24/156}$	$T_{30/150}$	$T_{45/135}$	$T_{50/130}$	B_{in}	B_{out}	A_{in}	A_{out}
1.0 ns	3.550	3.550	0.438	0.438	0	0	0.965	0.950
1.5 ns	2.195	2.195	0.575	0.575	0	0	0.650	0.500
19.0 ns	1.490	1.610	0.620	0.820	0.2525	0.2345	0.850	0.250

TABLE III. Target observables from a three-dimensional radiation hydrodynamic simulation (HYDRA) and from a `lasertram`/view factor calculation (VF) using the settings in Table II. The laser power and inner cone fraction are calculated post-backscatter. The emission cone fraction measures the amount of hohlraum emission due to the inner beam spots. All VF observables lie within HYDRA uncertainties, which come from temporal averaging of ±0.1 ns.

	1.0 ns		1.5 ns		19.0 ns	
	HYDRA	VF	HYDRA	VF	HYDRA	VF
Total Laser Power [TW]	9.9 ± 0.2	9.983	4.9 ± 0.4	4.592	313 ± 14	316.5
Inner Cone Fraction	0.64 ± 0.01	0.641	0.58 ± 0.01	0.576	0.52 ± 0.01	0.522
Emission Cone Fraction	0.32 ± 0.02	0.333	0.32 ± 0.01	0.318	0.15 ± 0.01	0.143
Hohlraum Radation Temperature [eV]	46 ± 3	45	66 ± 1	65	251 ± 2	252

[15] J. R. Rygg, O. S. Jones, J. E. Field, M. A. Barrios, L. R. Benedetti, G. W. Collins, D. C. Eder, M. J. Edwards, J. L. Kline, J. J. Kroll, O. L. Landen, T. Ma, A. Pak, J. L. Peterson, K. Raman, R. P. J. Town, and D. K. Bradley, Phys. Rev. Lett. **112**, 195001 (2014).

[16] N. Izumi *et al.*, Bull. Am. Phys. Soc. **58**, 203 (2013).

[17] R. H. H. Scott, D. S. Clark, D. K. Bradley, D. A. Callahan, M. J. Edwards, S. W. Haan, O. S. Jones, B. K. Spears, M. M. Marinak, R. P. J. Town, P. A. Norreys, and L. J. Suter, Phys. Rev. Lett. **110**, 075001 (2013).

[18] S. W. Haan, S. M. Pollaine, J. D. Lindl, L. J. Suter, R. L. Berger, L. V. Powers, W. E. Alley, P. A. Amendt, J. A. Futterman, W. K. Levedahl, M. D. Rosen, D. P. Rowley, R. A. Sacks, A. I. Shestakov, G. L. Strobel, M. Tabak, S. V. Weber, G. B. Zimmerman, W. J. Krauser, D. C. Wilson, S. V. Coggeshall, D. B. Harris, N. M. Hoffman, and B. H. Wilde, Physics of Plasmas **2**, 2480 (1995).

[19] B. K. Spears, M. J. Edwards, S. P. Hatchett, J. D. Kilkenny, J. P. Knauer, A. Kritcher, J. D. Lindl, D. Munro, P. Patel, H. F. Robey, and R. P. J. Town, Phys. Plasmas **21**, 042702 (2014).

[20] M. M. Marinak, R. E. Tipton, O. L. Landen, T. J. Murphy, P. Amendt, S. W. Haan, S. P. Hatchett, C. J. Keane, R. McEachern, and R. Wallace, Physics of Plasmas **3**, 2070 (1996).

[21] J. D. Moody, Bull. Am. Phys. Soc. **58**, 278 (2013).